Experimental and analytical investigation of concrete failure modes in strand lifting loops under inclined loads

Young-Hun Oh, Gang-Chul Lee, HyunSup Noh, Kyeong Woong Ra, NanHee Lee, and Jeong-Ho Moon

- Lifting loops are frequently used throughout production and transportation of precast concrete components; however, their design typically relies on simplified assumptions and engineering judgment.
- This paper discusses the finite element analysis and experimental study used to develop recommendations for design equations for lifting loops considering a range of edge distances, embedment depths, and lifting angles.
- Modification factors to established design equations are recommended to predict the strength of lifting loops in precast concrete components, and the equations were found to have good correlation with the experimental tests.

Precast concrete structures require lifting operations throughout their production, assembly, and installation stages. To facilitate these operations, lifting hardware is embedded within the concrete during manufacturing. Typically, factory-made anchor hardware or strands are employed for this purpose. While the specifications and performance of factory-produced anchor hardware are well-documented in manufacturers' brochures, the design and use of strands as lifting loops often uses simplified assumptions and engineering judgment, lacking a solid theoretical basis or rigorous experimental validation.

The design methods for using strands as lifting loops frequently rely on simplified assumptions. For instance, the design strength of a lifting loop is often calculated by multiplying an unverified bond stress by the embedment length. When loops are bent or hooked, the calculation often assumes that the entire length of the loop contributes equally to the strength, regardless of the loop's shape. This method leads to an overestimation of pullout strength, as the calculated strength increases proportionally with the total embedded length, whether the loop is bent or straight. Such practices can create safety blind spots and increase the risk of catastrophic failures.

The strand lifting loop (**Fig. 1**) offers flexibility by accommodating various conditions, such as embedment depth, edge or end distance, and lifting angle, to meet specific operational requirements. When the lifting angle is inclined (**Fig. 2**) rather than vertical (90 degrees) localized stress concentrations may

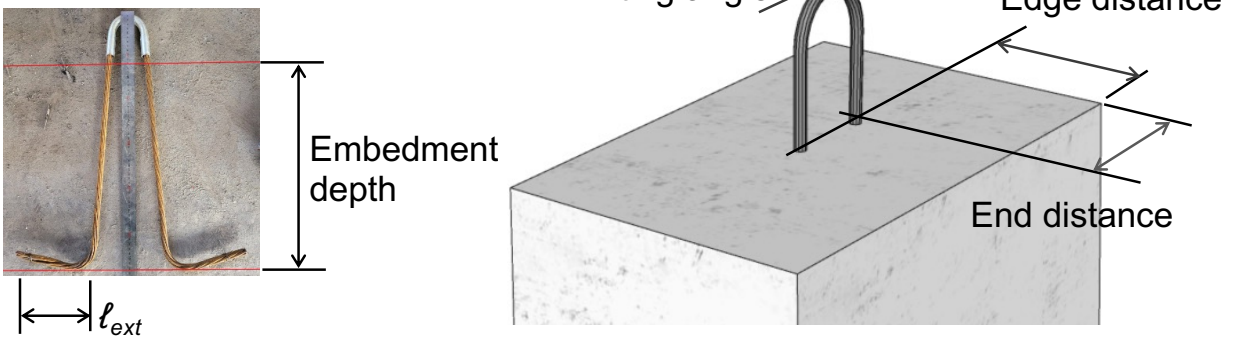

Figure 1. Strand lifting loop. Note: l_{ext} = length of strand loop extension (bend).

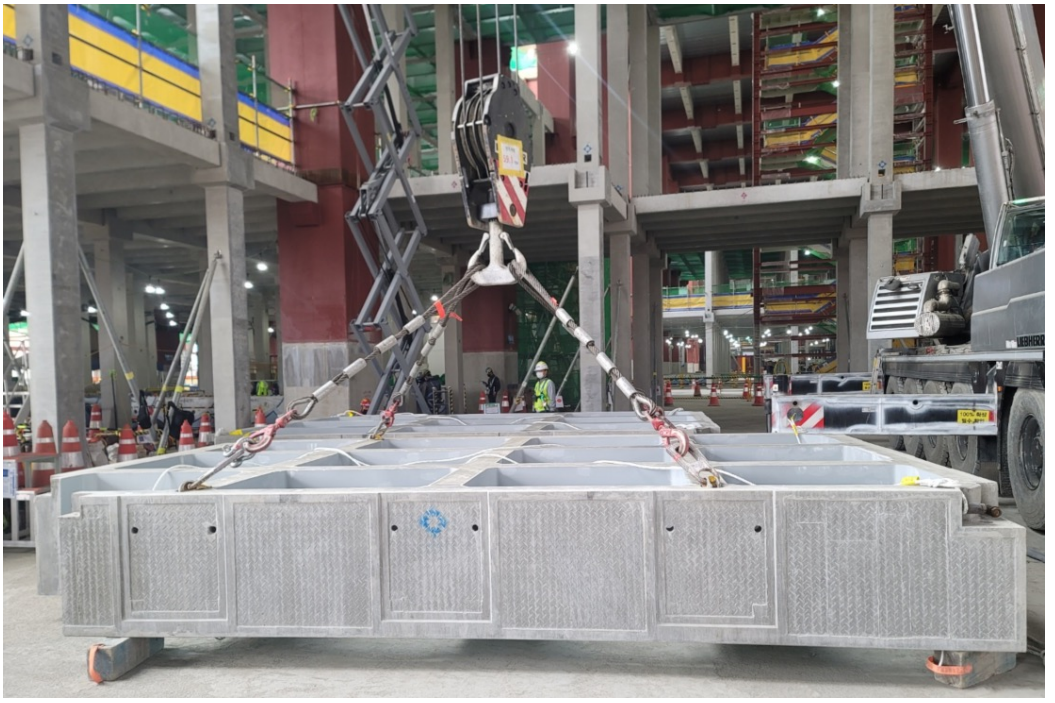

Figure 2. Inclined lifting of a precast concrete component. Photo courtesy of Samsung C & T Corp.

occur at the interface between the hardware and the concrete. The inherent flexibility of the strand helps alleviate these stress concentrations by permitting self-deformation.

A distinctive feature of strand lifting loops is that both legs of the strand bear the load together until failure occurs, at which point either one leg of the strand breaks or the surrounding concrete fails. Moreover, the ends of the strands embedded in the concrete are often bent into a hook shape, which distributes stress more evenly and improves resistance to failure modes such as concrete breakout.

The *PCI Design Handbook: Precast and Prestressed Concrete*[1] and the *PCI Bridge Design Manual*[2] have long provided design guidelines for the safe use of strand lifting loops in practice. These guidelines specify that the design load for strand lifting loops must ensure a safety factor of 4. This safety factor also requires that the straight sections of

the lifting loop legs be embedded at least 610 mm (24 in.). If the embedment depth is less than this, a 90-degree hook or broomed legs should be used; however, these manuals do not specify limitations for edge distance or end distance, focusing primarily on ensuring that the embedment depth exceeds a minimum value. In thin members, achieving the minimum embedment depth may not be feasible. Therefore, an evaluation of the failure modes and strength of the lifting loop under such conditions would be required. Moreover, when inclined loads (Fig. 2) are applied to the strand lifting loop, their effect on pullout strength must also be considered.

This study investigates effective methods for using strands as lifting loops in precast concrete structures. To achieve this, structural experiments and finite element analysis (FEA) were conducted to evaluate the effect of various critical variables on the performance of strand lifting loops. Based on the results of this research, a new design methodology was proposed, incorporating modification factors that account for the unique characteristics of strand lifting loops and enhance reliability. These factors were developed in accordance with the *Building Code Requirements for Structural Concrete (ACI 318-19) and Commentary (ACI 318R-19)*[3] design criteria for anchors, specifically addressing the strength of concrete failure mechanisms (for example, breakout) and the tensile fracture of the strand.

Previous research

Moustafa[4] conducted 272 experiments as part of the Concrete Technology Associates (CTA) program, focusing on critical variables such as embedment length, strand surface condition, strand diameter, and concrete strength. In these experiments, 16 strands were embedded at 150 mm (6 in.) intervals in a concrete block measuring 300 mm (12 in.) wide, 820 mm (32 in.) deep, and 3600 mm (140 in.) long. Each strand was tensioned sequentially, with embedment lengths of 300 mm, 460 mm (18 in.), 610 mm (24 in.), and 760 mm (30 in.). Based on the results of Moustafa's experiments, the *PCI Design Handbook*[1] recommends an embedment length of at least 610 mm for lifting loops, regardless of the strand shape.

The Illinois Department of Transportation sought to use strands as lifting loops for deck beams where the beam thickness was less than the 610 mm (24 in.) minimum embedment depth recommended by the *PCI Design Handbook*.[1] To evaluate the effects of reduced embedment depth, Kuchma and Hart[5] from the University of Illinois conducted a two-phase experimental study. In the first phase, 16 specimens with strand loops embedded in deck beams thinner than 610 mm were tested with varying lifting angles of 60 and 45 degrees. The reduced embedment depth resulted in failure governed by concrete fracture. The second phase focused on strand breakage, with specimens designed to ensure sufficient embedment depth. Variables in this phase included lifting angle, number of strands, and pullout method.

Chhetri et al.[6,7] from the University of Cincinnati conducted an experimental study on specimens using a 15.2 mm (0.6 in.) diameter strand as a lifting loop, based on industry survey results on the use of strand lifting loops among precast concrete manufacturers. The experiments involved pullout tests on loop-shaped strands embedded in large concrete blocks measuring 305 mm (12 in.) wide and 1120 mm (44 in.) long, with strands spaced at intervals twice the embedment depth. The study investigated loop shape (either straight or bent) and embedment depth, which ranged from 610 to 1070 mm (24 to 42 in.), exceeding the depth recommended by the *PCI Design Handbook*.[1] The observed failure modes included concrete blowout and strand pullout.

A review was conducted on 64 specimens from Moustafa's experiments using 12.7 mm (0.5 in.) diameter strands, 16 concrete failure-type specimens from Kuchma and Hart's experiments, and 13 specimens from Chhetri et al.'s study. These specimens are summarized in **Table 1**, and the distribution of strand stress at failure with respect to embedment depths is shown in **Fig. 3**, where the strand stress is calculated using twice the cross-sectional area of the strands for a two-leg strand configuration.

In Moustafa's experiments (CTA in Fig. 3), when the embedment depth exceeded 610 mm (24 in.), the stresses approached the failure stress of the strand f_{pu} of 1860 MPa (270 ksi). Even for bend-type strands (CTA-bend in Fig. 3) with embedment depths less than 610 mm, the stresses also approached f_{pu}. Based on these findings, the *PCI Design Handbook*[1] recommends a minimum embedment depth of 610 mm. The results marked with triangles on the left side of Fig. 3 represent

Table 1. Previous studies

Researcher	Strand shape	Strand end type	Number of specimens	Lifting angle, degrees	Embedment length, mm	Edge distance, mm	Failure mode
Moustafa (1974)	1 leg	straight	32	90	460, 610	150	slip fracture
		bend	32	90	300 to 760	150	slip fracture
Kuchma and Hart (2009)	2 leg	bend	16	45, 60	150 to 330	75 to 150	breakout
Chhetri et al. (2020, 2021)	2 leg	bend	5	90	610, 760	150	pullout blowout
		straight	8	90	810 to 1070	150	pullout blowout

Note: 1 mm = 0.0394 in.

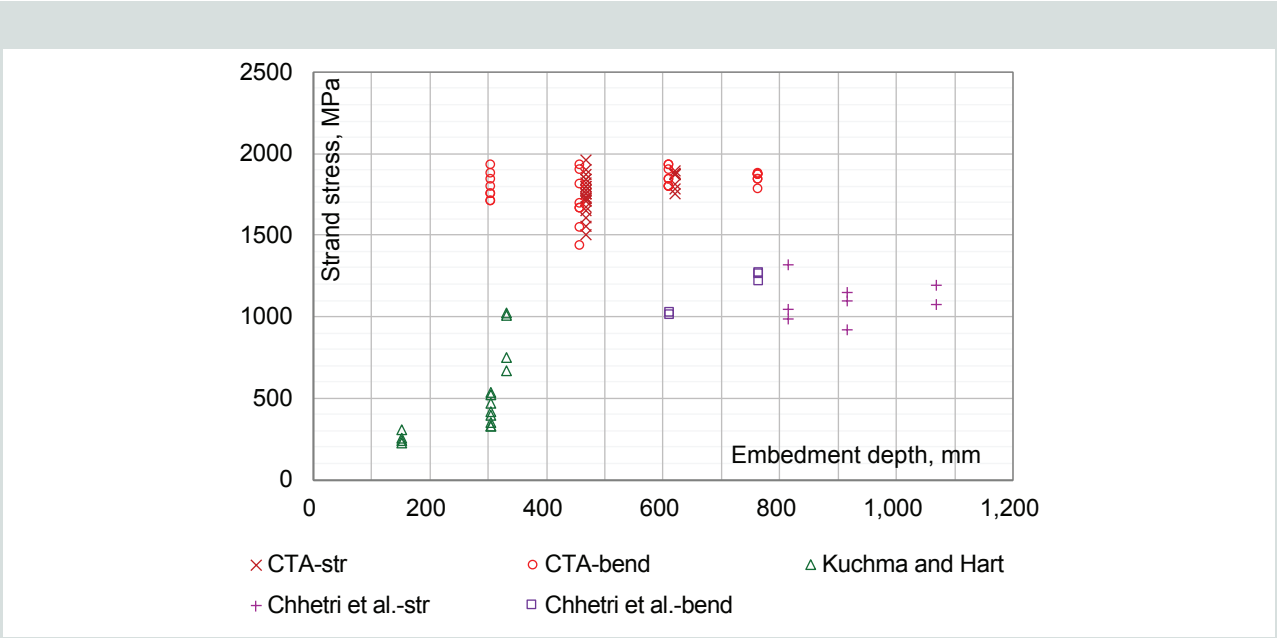

Figure 3. Previous tests. Note: Chhetri et al.-bend = bend-type strands tested in Chhetri (2020, 2021); Chhetri et al.-str = straight strands tested in Chhetri (2020, 2021); CTA-bend = bend-type strands tested in Moustafa (1974); CTA-str = straight strands tested in Moustafa (1974); Kuchma and Hart = Kuchma and Hart (2009). 1 mm = 0.0394 in.; 1 MPa = 0.145 ksi.

test specimens from Kuchma and Hart,[5] where strength was determined by concrete failure. These specimens had shallow embedment depths and the strand stress was lower than other tests at failure, indicating that their strength was governed by concrete failure rather than strand failure; however, the specimens with an embedment depth of 330 mm (13 in.) exhibited relatively higher stresses because the strands were embedded in high-strength concrete (64 MPa [9.2 ksi]).

Chhetri and Cross[8] investigated the effect of multiple-strand loops on pullout capacity. The study emphasized the importance of inserting a pipe or conduit sleeve to crush the strands before bending the multiple-strand loops. Furthermore, it demonstrated that the pullout strength of multiple-strand loops increases with embedment depth when the strands are evenly loaded. Based on these findings, Cross[9] explained the key revisions made to the *PCI Bridge Design Manual*.[2]

Although previous studies have extensively explored key variables, they often lack a comprehensive analysis of the relationships between these variables and the resulting outcomes. The failure mode may vary depending on the combination of embedment depth, edge distance, and lifting angle; however, clear guidelines for these variations are limited. In practice, the shapes of precast concrete members are highly diverse, and factors such as form removal and transportation substantially affect the design of lifting loops. Therefore, to facilitate the broader use of strand lifting loops, there is a need for a design method that can be mathematically formulated.

Experimental plan

The strand lifting loops can be used in various ways depending on the type of concrete component and the conditions at the factory or construction site, so all possible variations should be taken into account in the experiment. However, because it is impractical to include every possible variation as a variable in the experimental study, the experiment was designed to focus on key variables. The validity of the design was then evaluated through FEA and an analysis of the design requirements in ACI 318. In this process, both the strand and concrete failure behaviors were incorporated into the design equations by including the embedment depth, edge distance, and lifting angle as experimental variables.

Previous studies, such as those by Kuchma and Hart,[5] investigated lifting angles of 45 degrees (with conventional concrete) and 60 degrees (with high-strength concrete) with varying embedment depths; however, their research did not consider a range of edge or end distances, leading to conclusions that were specific to the needs of the Illinois Department of Transportation. Furthermore, most previous studies embedded multiple strands in a single concrete block, tensioning them sequentially. This method could not fully eliminate the influence of one pullout test on the surrounding concrete, potentially skewing the results of subsequent tests on other strands. To address this, each specimen in this study was designed to contain only one strand lifting loop per concrete block, ensuring that each test was independent.

This study involved a total of 24 specimens, with variables including edge distance ca, embedment depth h_{ef}, and lifting angle. **Table 2** lists the specimen variables organized by the edge distances of 85, 110, 160, and 210 mm (3.3, 4.3, 6.3, and 8.3 in.). Within each category, the specimens were further divided into two groups based on lifting angles of 45 and 60 degrees. For each lifting angle, three different embedment depths were selected as variables. The specimens were rectan-

Table 2. Specimen list

Name	Edge distance c_a, mm	Lifting angle, degrees	Embedment depth h_{ef}, mm	Thickness, mm	Height, mm
S-1	85	45	150	170	400
S-2			250		500
S-3			350		700
S-4		60	150	170	400
S-5			250		500
S-6			350		700
S-7	110	45	250	220	500
S-8			350		600
S-9			450		700
S-10		60	250	220	500
S-11			350		600
S-12			450		700
S-13	160	45	250	320	500
S-14			350		600
S-15			450		700
S-16		60	250	320	500
S-17			350		600
S-18			450		700
S-19	210	45	250	420	500
S-20			350		600
S-21			450		700
S-22		60	250	420	500
S-23			350		600
S-24			450		700

Note: 1 mm = 0.0394 in.

gular in shape, with thickness and height determined based on the edge distance and embedment depth.

The specimens were constructed using wooden formwork (**Fig. 4**). To control cracking, 10 mm (0.4 in.) diameter reinforcement was placed in a double layer with 150 mm (6 in.) spacing in both horizontal and vertical directions. The reinforcement was positioned as close to the edges as possible to control cracking without affecting the strength. The lifting loops were fabricated from 12.7 mm (0.5 in.) diameter strands of SWPC7B (7-wire prestressing strand) material with f_{pu} of 1860 MPa (270 ksi), and the concrete was designed with a compressive strength of 40 MPa (5.8 ksi). Material testing revealed that the concrete used in the specimens had an average compressive strength of 38.0 MPa (5.5 ksi).

For testing, the specimens were loaded by fixing them at inclines of 60 or 45 degrees (**Fig. 5**) and applying a vertical tensile force to the U-shaped protruding lifting loop. A steel rod was inserted into a polyvinyl chloride pipe embedded in the concrete before casting and bolted to the support for installation. To prevent localized forces from affecting the lifting loop, the loading area was wrapped with a U-shaped aluminum pipe (lifting eye) that matched the shape of the lifting loop. The tensile force was then transmitted to the specimen through a steel round rod with a diameter of 50 mm (2 in.).

Verification of experimental conditions

To evaluate whether the specimen's size, shape, loading method, and support conditions were suitable for the experi-

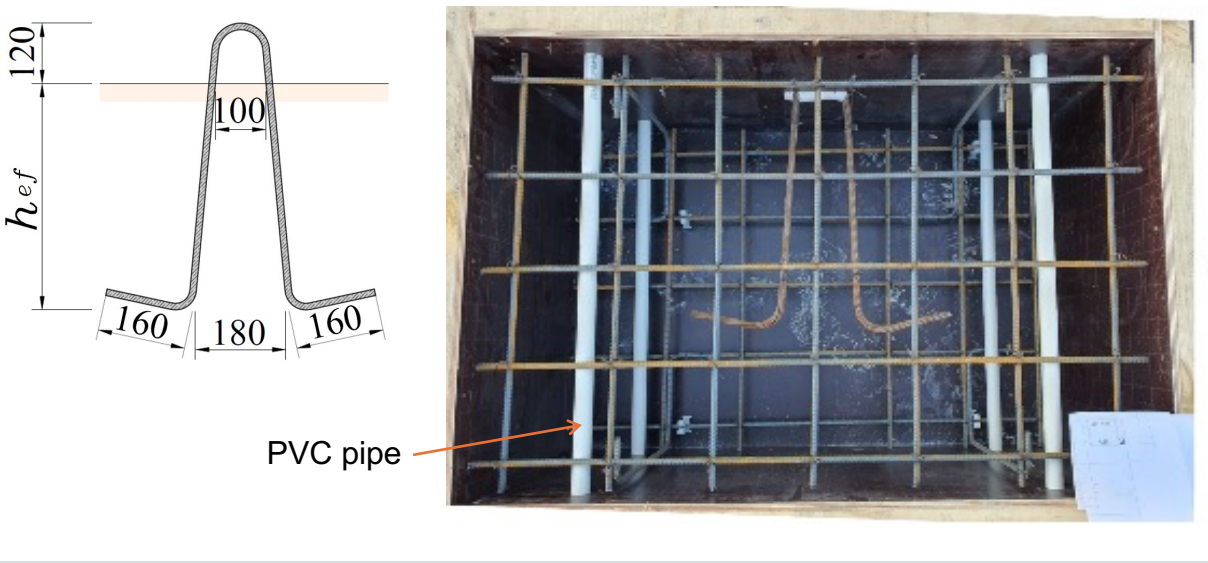

Figure 4. Shape and fabrication of lifting loop for specimen. Note: All units are in millimeters. h_{ef} = embedment depth of strand lifting loops; PVC = polyvinyl chloride. 1 mm = 0.0394 in.

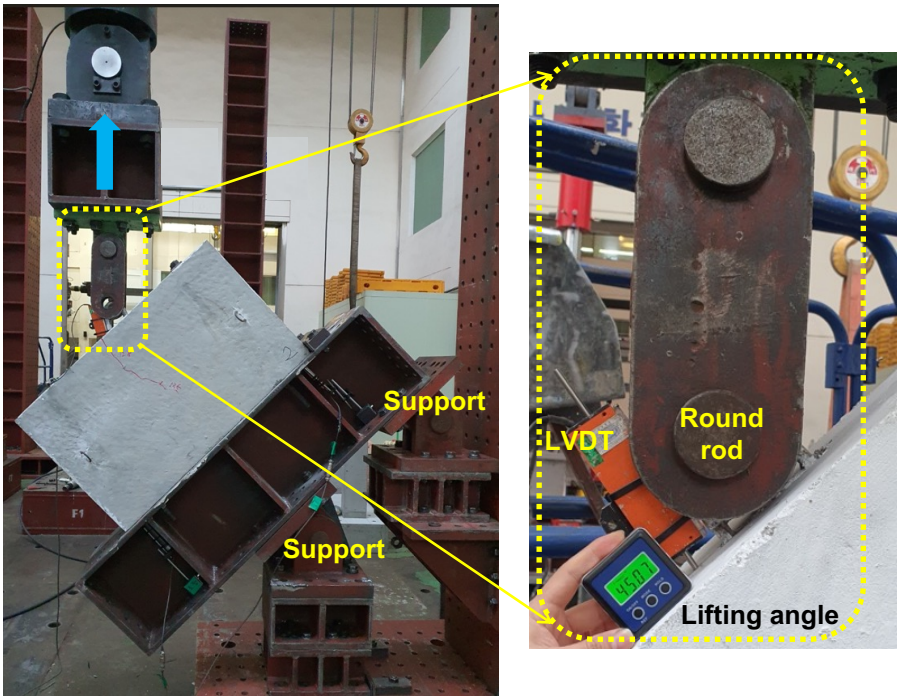

Figure 5. Test setup. Note: LVDT = linear variable displacement transducer.

mental objectives, an FEA was conducted. Specimen S-5 (with an embedment depth h_{ef} of 250 mm [10 in.], an edge distance c_a of 85 mm [3.3 in.], and a lifting angle of 60 degrees) was selected for this analysis, and linear analysis was performed using finite element analysis software. The FEA model (**Fig. 6**) was constructed using 8-node hexahedral elements, with automatic mesh generation ensuring a maximum element size less than 10 mm (0.4 in.). The analysis model included reinforcing bars with a diameter of 10 mm (D10), placed in double layers at 150 mm (6 in.) intervals in both vertical and horizontal directions, along with a 12.7 mm (0.5 in.) diameter strand loop. Considering symmetry, only half of the specimen was modeled (Fig. 6).

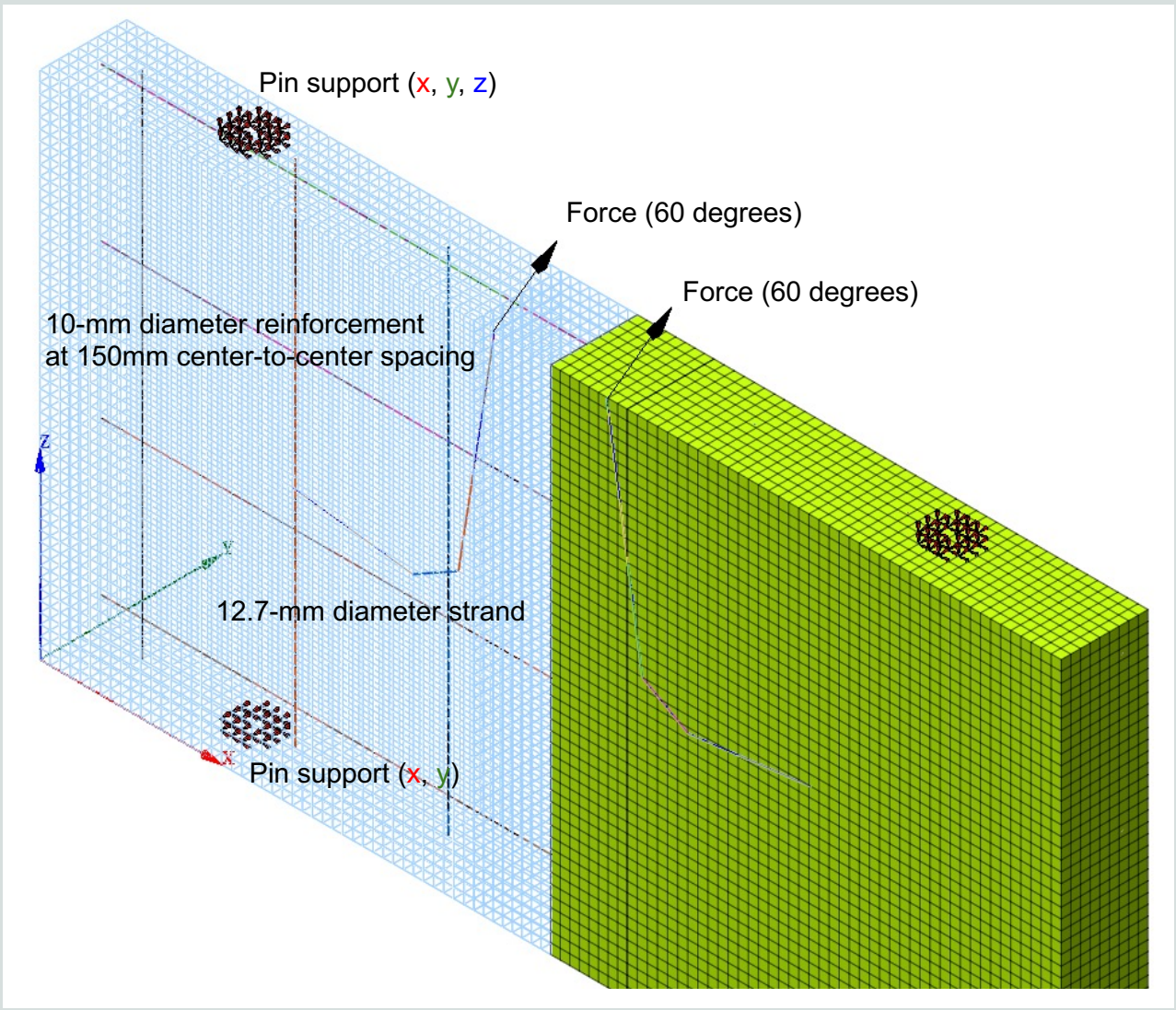

Figure 6. Finite element model. Note: 1 mm = 0.0394 in.

The material properties of the concrete were defined with an elastic modulus of 30,000 MPa (4350 ksi) and a Poisson's ratio of 0.17. The elastic modulus of the strands and reinforcing bars was chosen to be 200,000 MPa (29,000 ksi). A tensile force was applied at the point where each leg of the strand loop begins to embed. The magnitude of each tensile force corresponded to the maximum strength of a single strand. Because the specimen was fixed using steel rods with threaded ends fastened by bolts and washers, the support conditions were modeled as pin supports at the contact areas between the washers and the specimen. The upper surface contact areas were constrained with pin supports in the x, y, and z directions, while the bottom surface contact areas were constrained in the x and y directions due to the upward tensile load applied to the specimen.

The specimen was analyzed under three different conditions:

- with both reinforcing bars and strands (case 1)
- with only strands and no reinforcing bars (case 2)
- concrete only (case 3)

Figure 7 illustrates the distribution of principal tensile strain ε_{c1} and principal compressive strain ε_{c3} in the concrete, obtained from the analysis for case 1 and case 3. The principal tensile strain distributions are shown for the entire specimen, while the principal compressive strain distributions are presented only for the upper surface. Because the difference between case 2 and case 3 was negligible, only case 1 and case 3 are shown in the figure. To improve visualization and prevent strain distribution in less-concentrated areas from becoming invisible due to the large strain concentrations near the loading points, areas with high stress concentrations were hidden. Figure 7 shows that the principal strain distribution in concrete exhibited almost no difference, regardless of the presence of strands or reinforcing bars. At the support points, the strain remained localized with minimal propagation

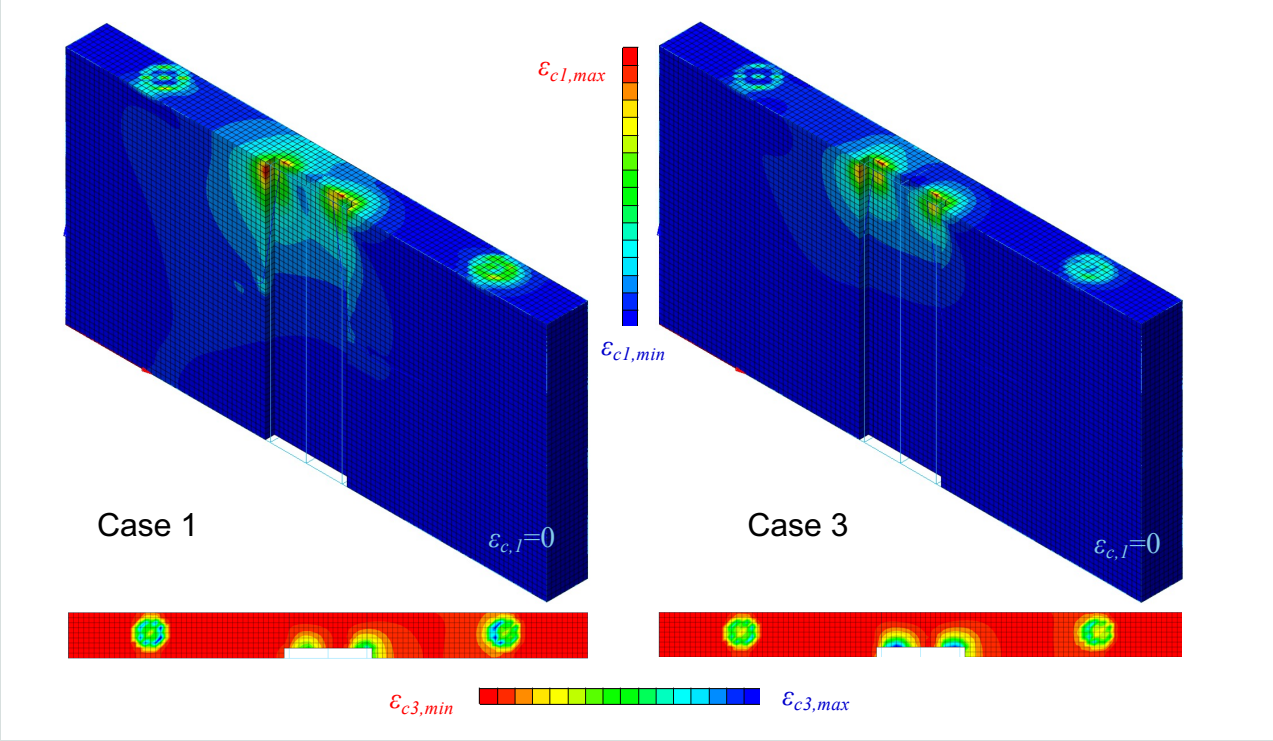

Figure 7. Principal strain distributions in concrete. Note: $\varepsilon_{c1,max}$ = maximum principal tensile strain; $\varepsilon_{c1,min}$ = minimum principal tensile strain; $\varepsilon_{c3,max}$ = maximum principal compressive strain; $\varepsilon_{c3,min}$ = minimum principal compressive strain.

beyond the area directly around the supports. In addition, in the region where the steel rod passed through, the strain approached zero, indicating that the steel rod had a negligible effect on the specimen's overall strength.

Figure 8 presents the distribution of stress in the strand σ_{ps} and reinforcing bar σ_s obtained from case 1, along with their maximum and minimum values. The results show that the maximum stress in the reinforcing bar was less than approximately 7% of that in the strand, indicating a much lower contribution from the reinforcing bars. Therefore, even in the event of specimen failure, the reinforcing bars are expected to have minimal impact on the load-carrying capacity. If the reinforcing bars do not yield, their contribution is considered to be limited to an increase in the transformed sectional area, proportional to the elastic modulus ratio between concrete and steel.

Specimen S-17 (with an embedment depth h_{ef} of 350 mm [14 in.], and edge distance c_a of 160 mm [6.3 in.], and a lifting angle of 60 degrees) was also analyzed to examine whether similar results are obtained when the edge distance or embedment depth varies. The results showed that the distribution of principal tensile and principal compressive strains in the concrete exhibited a trend very similar to that of specimen S-5. When no strand or reinforcement was present, the principal tensile strain tended to concentrate somewhat near the load point. In contrast, when the strand or reinforcement were present, the strain tended to spread more. However, as seen in Fig. 7, this tendency was not significant. On the other hand, the stress in the reinforcement was found to be considerably lower for S-17 compared with S-5. The maximum stress for specimen S-17 decreased to approximately one-fourth of the tensile stress and one-fifth of the compressive stress compared with specimen S-5. This suggests that as the thickness of the specimen increases, the influence of the reinforcement is expected to decrease.

Test results and evaluation

The experimental results were analyzed by evaluating the relationship between failure modes and the strength of the specimens. To facilitate this analysis, specimens with the same embedment depth were grouped together, and the cracking patterns observed on the upper surfaces of the specimens in each group are illustrated in **Fig. 9** through **11**.

The figures show that the failure modes of the specimens can be categorized as follows: tensile failure of the strand (TF), marked by circular dashed lines in the figures, breakout failure of the concrete (BR), indicated by rectangular dashed lines, and splitting rupture of the concrete (SP), which is not specifically marked. Tensile failure of the strand refers to the failure mode where the strand fractures at the maximum load. Breakout failure of the concrete is characterized by cracks that initiate near the strand and spread diagonally, ultimately causing the side to break out. Splitting rupture of the concrete is defined as the failure mode where the cracks do not prog-

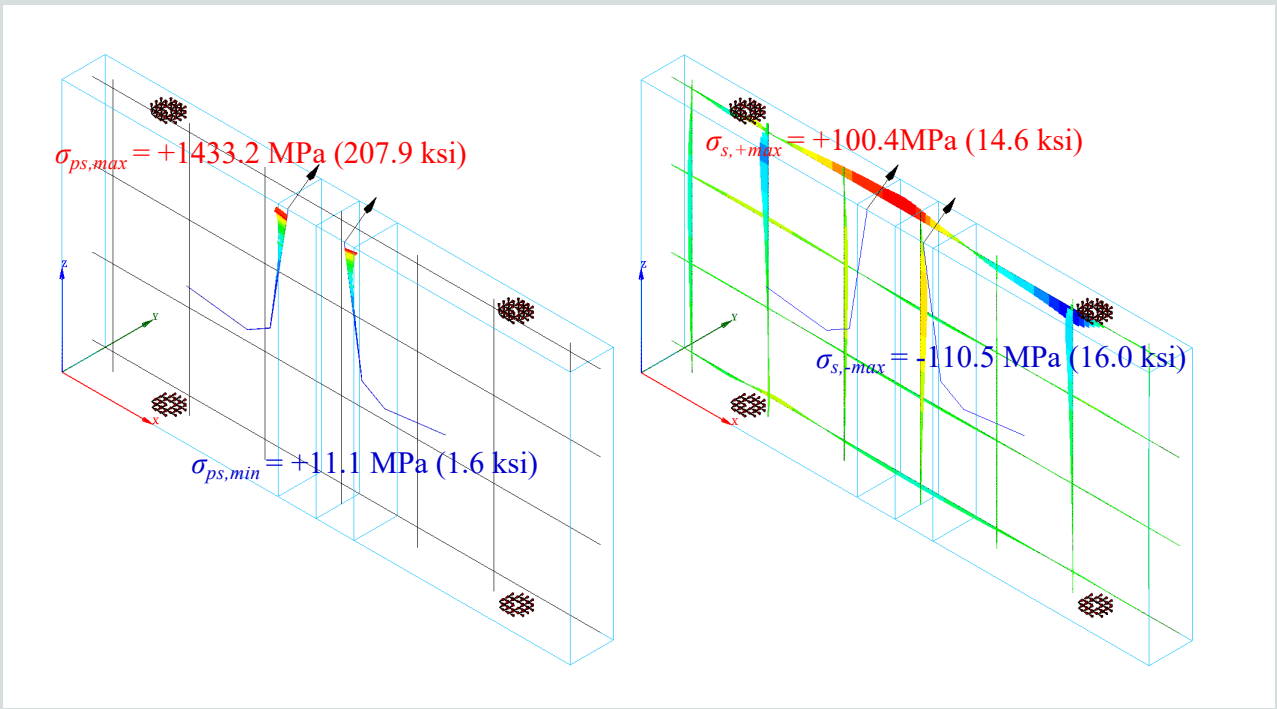

Figure 8. Stresses in the strands and reinforcing bars for case 1. Note: $\sigma_{ps,max}$ = maximum stress in the strand; $\sigma_{ps,min}$ = minimum stress in the strand; $\sigma_{s,+max}$ = maximum tensile stress in the reinforcing bar; $\sigma_{s,-max}$ = minimum compressive stress in the reinforcing bar. 1 MPa = 0.145 ksi.

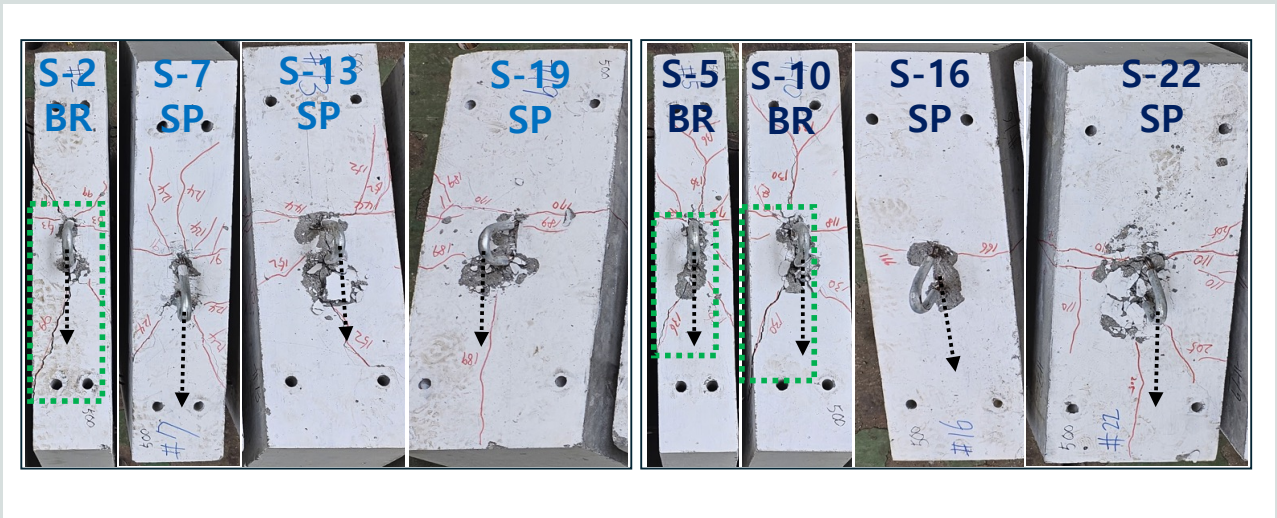

Figure 9. Failure modes (embedment depth of 250 mm). BR = breakout failure of the concrete; S-2 = specimen 2; S-5 = specimen 5; S-7 = specimen 7; S-10 = specimen 10; S-13 = specimen 13; S-16 = specimen 16; S-19 = specimen 19; S-22 = specimen 22; SP = splitting rupture of the concrete. Note: 1 mm = 0.0394 in.

ress to a breakout failure. Therefore, BR refers to the extended form of splitting failure.

In all specimens, except those that exhibited TF, SP cracks first appeared on the rear side of the loading point, followed by BR mode occurring on the front side of the loading point in some specimens. Because the specimens were loaded in an inclined direction (**Fig. 12**) the front and rear of the lifting loop can be distinguished by the bent shape of the loop in the photographs. The trend in failure modes observed during the experiments correlated with the FEA results, which showed that principal tensile stresses were greater on the rear side of the loading point, and principal compressive stresses were greater on the front side. This suggests that SP mode cracks occurred on the

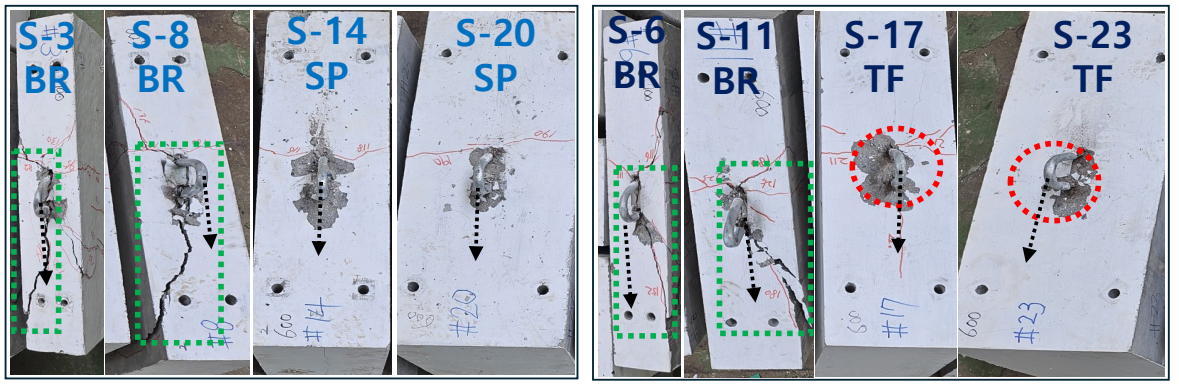

Figure 10. Failure modes (embedment depth of 350 mm). BR = breakout failure of the concrete; S-3 = specimen 3; S-6 = specimen 6; S-8 = specimen 8; S-11 = specimen 11; S-14 = specimen 14; S-17 = specimen 17; S-20 = specimen 20; S-23 = specimen 23; SP = splitting rupture of the concrete; TF = tensile failure of the strand. Note: 1 mm = 0.0394 in.

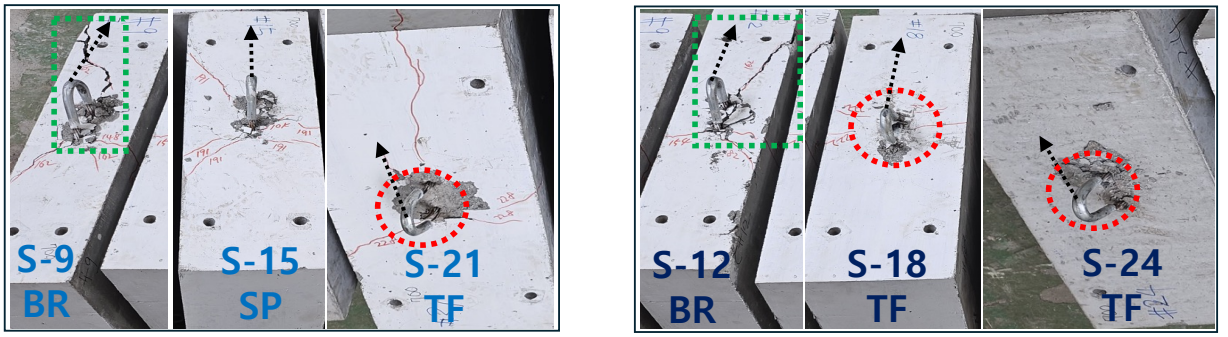

Figure 11. Failure modes (embedment depth of 450 mm). BR = breakout failure of the concrete; S-9 = specimen 9; S-12 = specimen 12; S-15 = specimen 15; S-18 = specimen 18; S-21 = specimen 21; S-24 = specimen 24; SP = splitting rupture of the concrete; TF = tensile failure of the strand. Note: 1 mm = 0.0394 in.

rear side due to principal tensile stress, while the combination of tensile and compressive stresses on the front side led to diagonal cracks progressing to BR mode failure.

Figures 13 and **14** illustrate the load-displacement relationships of the specimens. Because all specimens showed a rapid decrease in load-bearing capacity after reaching their peak load, only data up to that point are presented in the figures. The results show that specimens with smaller edge distances (S-1–S-12 in Fig. 13) exhibited only SP and BR modes, while those with larger edge distances (S-13–S-24 in Fig. 14) exhibited SP and TF modes, without the BR mode. This suggests that with sufficient embedment depth and larger edge distances, the specimen's strength may be determined by the TF mode, with no occurrence of the BR mode. Additionally, from Fig. 13, it can be observed that the strength of the SP mode specimens tends to be lower than that of the BR mode specimens.

Table 3 presents the failure modes, test strengths, and vertical components of strength for each specimen. The table shows that when the lifting angle was 60 degrees, specimens failed in TF mode if the edge distance was greater than or equal to 160 mm (6.3 in.) and the embedment depth was greater than or equal to 350 mm (14 in.). Similarly, when the lifting angle was 45 degrees, specimens failed in TF mode if the edge distance was greater than or equal to 210 mm (8.3 in.) and the embedment depth was greater than or equal to 450 mm (18 in.). Among the specimens in TF mode, S-17 and S-18, which had smaller edge distances, and S-21, which had a smaller lifting angle of 45 degrees but a larger edge distance, showed SP mode crack patterns before tensile failure. In contrast, S-23 and S-24, which had larger edge distances and a lifting angle of 60 degrees, did not exhibit crack patterns like the SP mode. Specimens with shallow embedment depths exhibited lower strength and failed in SP mode, even with increased lifting angles.

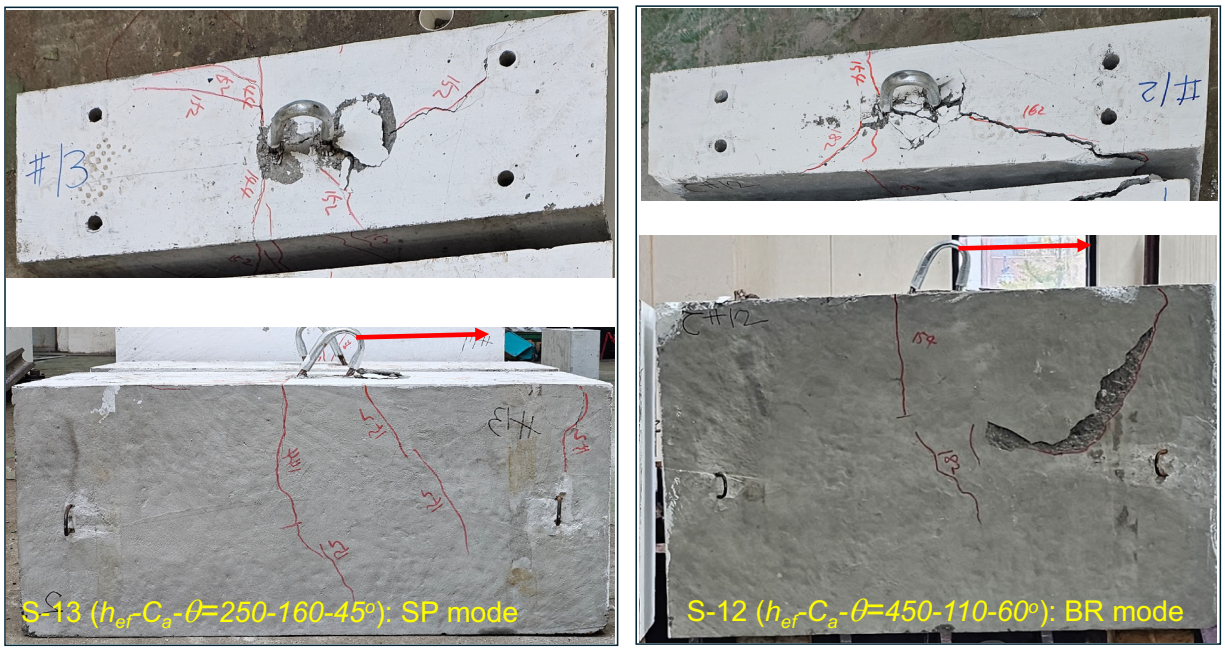

Figure 12. Example of failure modes: splitting rupture and breakout failure of concrete. Note: BR = breakout failure of the concrete; S-12 = specimen 12; S-13 = specimen 13; SP = splitting rupture of the concrete.

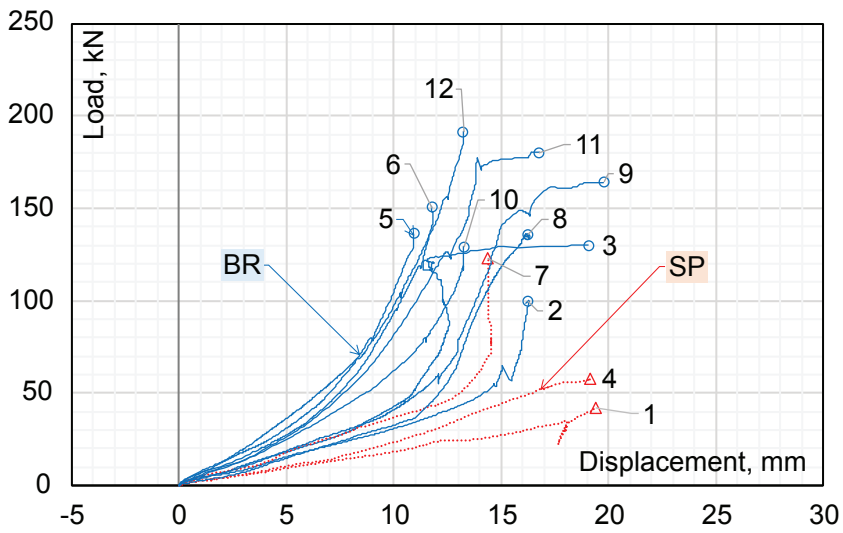

Figure 13. Load-displacement relationships for specimens S-1–S-12. Note: BR = breakout failure of the concrete; SP = splitting rupture of the concrete. 1 mm = 0.0394 in.; 1 kN = 0.225 kip.

For example, S-22, with a lifting angle of 60 degrees and an embedment depth of 250 mm (10 in.), failed in SP mode, while S-21, with a lifting angle of 45 degrees and an embedment depth of 450 mm, failed in TF mode. These observations underscore the importance of analyzing strength variations with respect to key parameters (edge distance, embedment depth, lifting angle).

To further analyze these variables, **Fig. 15** depicts the distribution of the specimens' strength ratio at different embedment depths. The vertical axis represents the strength ratio, which is the vertical component of the experimental load divided by the tensile strength of a single strand (test/$A_{ps}f_{pu}$). The figure reveals that specimens with a lifting angle of 45 degrees exhibited lower strength ratios compared to those with a

lifting angle of 60 degrees. In addition, when the embedment depth was constant, the strength of the specimens increased as the lifting angle increased (for example, comparing S-2 to S-5, S-7 to S-10, S-13 to S-16, and S-19 to S-22). However, it was observed that the strength of S-5 was slightly higher than that of S-10. Both specimens had the same lifting angle and embedment depth, so the strength of S-10, which had a larger edge distance, should have been higher. This anomaly could be attributed to variability in the concrete test data. Aside from this case, no other such exceptions were observed. Among specimens with a lifting angle of 60 degrees, those with an embedment depth of 350 mm (14 in.) or more (S-17, S-18, S-23, S-24) failed in TF mode. Similarly, among specimens with a lifting angle of 45 degrees, S-21, with an embedment depth of 450 mm (18 in.), failed in TF mode. However, because the strength was converted to its vertical component, the strength ratio of S-21 appears lower.

Figure 16 presents the strength ratio distribution of the specimens based on edge distance. This figure also indicates that the strength ratio increased as the edge distance increased. Specimens with a lifting angle of 45 degrees had lower

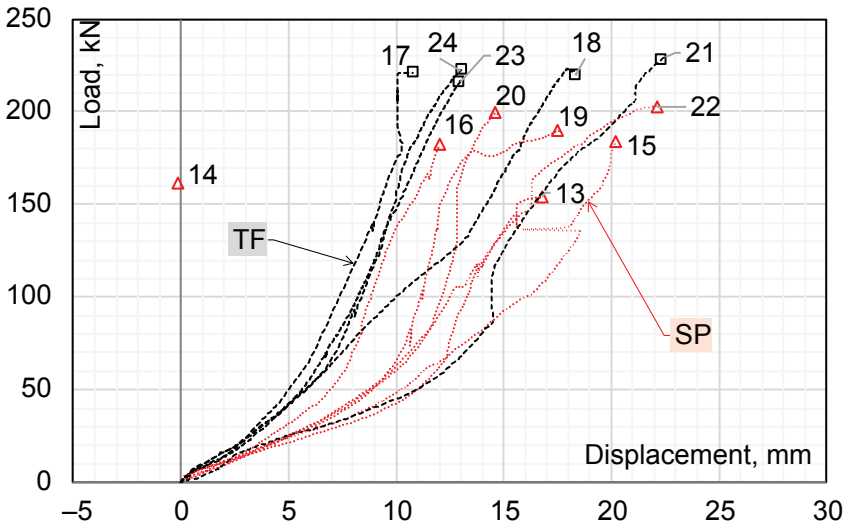

Figure 14. Load-displacement relationships for specimens S-13–S-24. Note: SP = splitting rupture of the concrete; TF = tensile failure of the strand. 1 mm = 0.0394 in.; 1 kN = 0.225 kip.

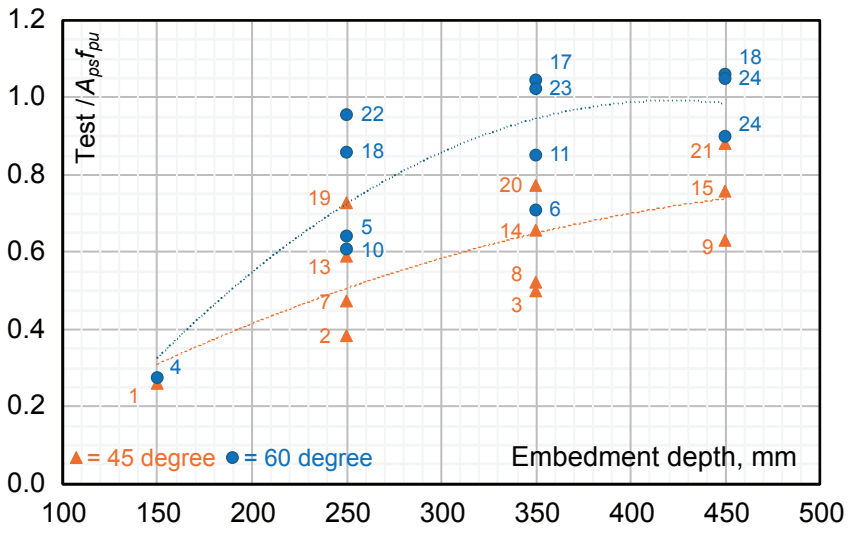

Figure 15. Strength ratio at different embedment depths. Note: test/$A_{ps}f_{pu}$ = vertical component of the experimental load divided by the tensile strength of a single strand. 1 mm = 0.0394 in.

Table 3. Failure modes and strength of specimens

Name	Edge distance c_a, mm	Lifting angle, degrees	Embedment depth h_{ef}, mm	h_{ef}/c_a	Failure mode	Test strength, kN	Vertical strength, kN
S-1	85	45	150	1.76	SP	67.7	47.9
S-2			250	2.94	BR	99.9	70.6
S-3			350	4.12	BR	130.0	91.9
S-4		60	150	1.76	SP	58.1	50.3
S-5			250	2.94	BR	136.4	118.1
S-6			350	4.12	BR	150.8	130.6
S-7	110	45	250	2.27	SP	123.4	87.2
S-8			350	3.18	BR	136.1	96.2
S-9			450	4.09	BR	164.0	115.9
S-10		60	250	2.27	BR	129.2	111.9
S-11			350	3.18	BR	180.7	156.5
S-12			450	4.09	BR	191.4	165.7
S-13	160	45	250	1.56	SP	153.7	108.7
S-14			350	2.19	SP	170.4	120.5
S-15			450	2.81	SP	196.9	139.2
S-16		60	250	1.56	SP	182.1	157.7
S-17			350	2.19	TF	222.4	192.6
S-18			450	2.81	TF	225.3	195.1
S-19	210	45	250	1.19	SP	189.7	134.2
S-20			350	1.67	SP	200.8	142.0
S-21			450	2.14	TF	229.3	162.2
S-22		60	250	1.19	SP	203.0	175.8
S-23			350	1.67	TF	217.6	188.4
S-24			450	2.14	TF	222.7	192.9

Note: BR = breakout failure of the concrete; SP = splitting rupture of the concrete; TF = tensile failure of the strand. 1 mm = 0.0394 in.; 1 kN = 0.225 kip.

strength ratios than those with a lifting angle of 60 degrees. Furthermore, except for TF mode, the strength of specimens increased with greater embedment depths when the edge distance was constant (for example, comparing S-7, S-8, and S-9 and comparing S-10, S-11, and S-12).

Failure modes and influence factors

This study examined the effects of embedment depth, edge distance, and lifting angle of strand lifting loops on the strength and failure modes through experimentation. To develop a design formula based on these results, it is crucial to establish correlations between the key variables and the strength of the test specimens. Various evaluation analyses revealed that the ratio of embedment depth to edge distance h_{ef}/c_a (referred to here as the influence factor) was significantly associated with the failure modes of the test specimens. Table 3 shows that when the influence factor is 3.0 or less, the failure mode is generally classified as SP, while it tends to be classified as BR when the influence factor exceeds 3.0.

Figure 17 presents the influence factor values (vertical axis) for each specimen (horizontal axis) and also indicates the failure mode. In the figure, a triangular marker represents SP, a circular marker represents BR, and a square marker represents TF. Additionally, unfilled markers indicate a lifting angle of 45 degrees, while filled markers indicate a lifting angle of 60 degrees. The figure shows that within groups of specimens with the same edge distance (for example, 1–3, 4–6, 7–9), as the influence factor increases, the failure mode

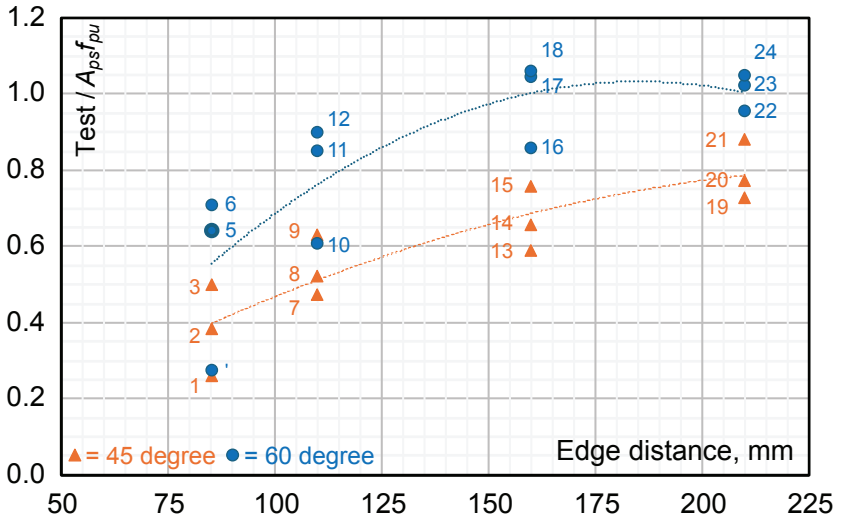

Figure 16. Strength ratio at different edge distances. Note: test/$A_{ps}f_{pu}$ = vertical component of the experimental load divided by the tensile strength of a single strand. 1 mm = 0.0394 in.

shifts from SP to BR. This indicates that even with the same edge distance, a deeper embedment depth can lead to a shift to BR mode. It can be inferred that as the embedment depth increases, the load-resistance capacity increases, allowing the specimen to withstand greater loads, resulting in BR mode cracks forming at the front of the loading point, where principal compressive stresses are high. This suggests that the strength is likely to increase as the influence factor increases.

It is also noteworthy that specimens with a lifting angle of 60 degrees and an edge distance of 110 mm (4.3 in.) (specimens S-10–S-12) all exhibited the BR mode, whereas specimens with a lifting angle of 45 degrees and a larger edge distance of 160 mm (6.3 in.) (specimens S-13–S-15) all exhibited the SP mode. This suggests that even with an increased edge distance, a smaller lifting angle may result in the SP mode rather than the BR mode.

For specimens with an edge distance of 160 mm (6.3 in.) or more and a lifting angle of 60 degrees (specimens S-16–S-18, S-22–S-24) and those with an edge distance of 210 mm (8.3 in.) or more and a lifting angle of 45 degrees (specimens S-19–S-21), the failure mode shifted directly from SP to TF as the embedment depth increased. This indicates that the failure mode of the specimens showed a consistent pattern depending on edge distance, embedment depth, and lifting angle.

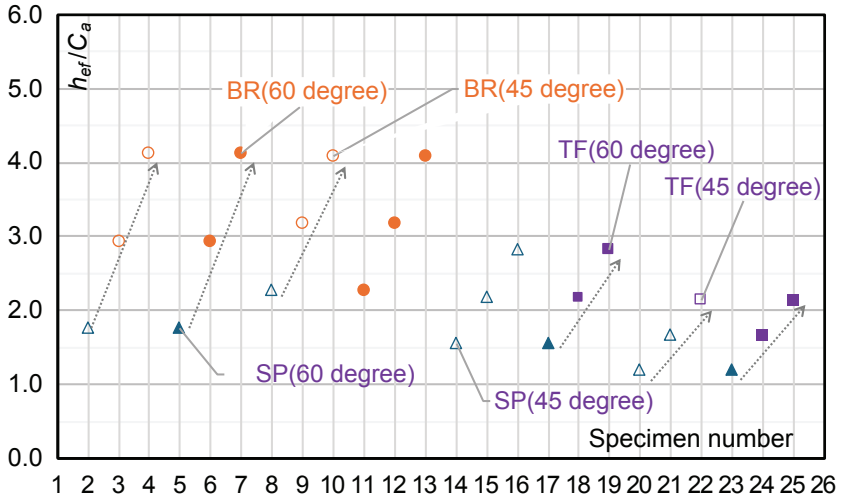

Figure 17. Influence factor by specimen number. Note: BR = breakout failure of the concrete; c_a = edge distance of strand lifting loops; h_{ef} = embedment depth of strand lifting loops; SP = splitting rupture of the concrete; TF = tensile failure of the strand.

If the failure modes of the test specimens can be classified into concrete failure modes such as SP and BR and strand failure modes such as TF, this would align with the failure mode classification in the design method for anchors in ACI 318. The ACI code suggests different methods for calculating the strength of the anchor based on whether the failure mode is in steel or concrete.

The failure modes of the test specimens are not significantly different from those of the anchor design in ACI 318, although the stress distribution around the strand might differ due to the geometric differences of the lifting loop. As mentioned before, the two-leg strand lifting loop in a bent shape can spread the stress more widely. Therefore, it can be proposed that the strand lifting loop can be designed in a manner similar to the ACI 318 design requirements for anchors. If the characteristics of the strand lifting loop can be incorporated, a design method for the strand lifting loop could be developed.

Proposed modification to ACI 318 method

To determine the structural characteristics of strand lifting loops, this study evaluated how the experimental strength distribution aligns with the design method outlined in ACI 318. The strength of the specimens was calculated using the anchor design method from ACI 318, and these results were compared with experimental outcomes.

ACI 318 categorizes the failure modes of anchors subjected to tensile forces into steel failure and concrete failure to determine the design strength. Steel failure modes include the tensile failure of the anchor, while concrete failure modes encompass breakout, pullout failure, side-face blowout for headed anchors, and bond failure for adhesive anchors. In cases like the one examined in this study, where strands are used with a lifting loop, the critical failure modes may include the tensile failure of the strand and concrete breakout.

The anchor design method outlined in ACI 318 calculates the nominal tensile strength for the tensile failure of anchor steel as follows:

$$N_{sa} = A_{se,N} f_{uta} \tag{1}$$

where

$A_{se,N}$ = effective cross-sectional area of the anchor in tension

f_{uta} = specified tensile strength of anchor steel

For the breakout failure mode of anchors subjected to tensile forces, the nominal tensile strength N_{cbg} is calculated by multiplying the basic breakout strength of a single anchor by correction factors. Correction factors include the eccentricity factor $\Psi_{ec,N}$, edge effect factor $\Psi_{ed,N}$, cracking factor $\Psi_{c,N}$, and splitting factor $\Psi_{cp,N}$.

$$N_{cbh} = \frac{A_{Nc}}{A_{Nco}} \Psi_{ec,N} \Psi_{ed,N} \Psi_{c,N} \Psi_{cp,N} N_b \tag{2}$$

where

A_{Nc} = projected concrete failure area of a single anchor or group of anchors

A_{Nco} = projected concrete failure area of a single anchor for calculation of strength in tension

N_b = basic concrete breakout strength

Given that the influence factor showed a noticeable correlation with failure modes, a relationship between the strength ratio (y-axis) and the influence factor (x-axis) was plotted, with trend lines included for different lifting angles (**Fig. 18**). Because the expected strength in ACI 318 is the vertical strength, the vertical component of the specimen strength was divided by the expected strength to obtain the strength ratio. To derive the trend lines, only specimens that failed by concrete failure were included, excluding those that failed by TF mode. As a result, trend lines were obtained for lifting angles of 60 and 45 degrees. The trend lines indicated that the strength ratio tended to increase as the influence factor increased. Additionally, the trend lines for the 60- and 45-degree lifting angles showed different tendencies, with the strength ratio being lower for smaller lifting angles.

The observation that the strength ratio increases with the influence factor (Fig. 18) suggests that the influence factor can be incorporated into the equation for estimating the strength of specimens. Therefore, it was determined that by using the trend line as a modification factor, it might be possible to obtain an estimated strength that better matches the experimental strength while reflecting the effect of the influence factor. In this study, the following modification factors, shown in Eq. (3) and (4), were proposed:

For strand failure (TF):

$$\Psi_\beta = \alpha \tag{3}$$

where

α = factor accounting for lifting angle of strand lifting loops in ACI anchor design

Ψ_β = strength modification factor

For concrete failure (SP or BR):

$$\Psi_\beta = \alpha \left(0.35 \times \frac{h_{ef}}{c_a} \right) + 0.4 \le 1.5 \tag{4}$$

where

c_a $\geq$ 85 mm

$\frac{h_{ef}}{c_a}$ $\geq$ 5.0

In Eq. (3) and (4), a factor accounting for lifting angle of strand lifting loops in ACI anchor design α of 0.7 is applied

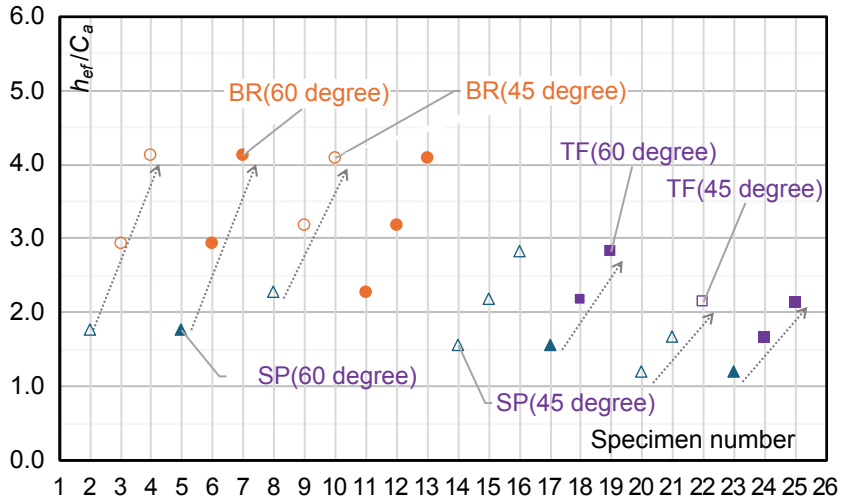

Figure 18. Trends in test/ACI values by influence factor. Note: ACI = ACI (2019); c_a = edge distance of strand lifting loops; h_{ef} = embedment depth of strand lifting loops.

for a lifting angle of 45 degrees, and a factor accounting for lifting angle of strand lifting loops in ACI anchor design α of 1.0 is used for a lifting angle of 60 degrees or more. The value in Eq. (4) is limited to 1.5 or less because the test results were derived from a limited number of specimens, so the limit was set to ensure safety. The influence factor was also limited to 5.0 or less because the influence factors for the specimens in this study did not exceed 5.0. The effect of the lifting angle was incorporated into the equations because the strength ratio for specimens with a 45-degree lifting angle was lower (Fig. 15 and 16) than the strength ratio for specimens with a 60-degree lifting angle. For lifting angles between 45 and 60 degrees, a linearly interpolated value can be used, and the effect of the lifting angle is recommended to be applied to specimens that failed by TF mode. **Figure 19** shows the distribution of Eq. (4) compared with experimental results and trend lines from Fig. 18.

By using Eq. (3) and (4) to modify the design strength in ACI 318, it becomes possible to derive consistent design equations for strand lifting loops. **Figure 20** shows that the ratio of experimental strength to predicted strength ranges from 0.99 to 1.67, with an average value of 1.17 (a coefficient of variation [COV] of 15%). Because the anchor design in ACI 318 is based on a large database, using this as a foundation and incorporating modification factors that account for the characteristics of strand lifting loops results in valid design equations.

The proposed equations were also applied to the specimens from Kuchma and Hart,[5] which included concrete failure rather than strand failure. In **Table 4**, the strength ratio represents the ratio of experimental strength to expected strength.

In **Fig. 21**, both the experimental specimens from this study and those from Kuchma and Hart[5] are presented on the same graph. The figure shows that the strength ratios (defined as the ratio of experimental strength to expected strength) generally approach the expected strength, except in cases where the strength ratio is significantly higher, around 3.0, for specimens with three strands and a 60-degree angle (I-13 to I-16). Specimens with a small edge distance of 75 mm (3 in.) (represented by unfilled markers) exhibited lower strength ratios, indicating that they fall outside the proposed formula's application range of 85 mm (3.3 in.). The higher strength ratios for specimens with more strands could be attributed to a larger contact area with the concrete. Additionally, it is possible that specimens I-13 to I-16 were constructed with high-strength concrete (64 MPa [9.3 ksi]) and included vertical stirrups, which may have contributed to the observed differences. Excluding the specimens with three strands and a 60-degree angle, the average strength ratio was 1.21 (a COV of 30%), which is similar to the 1.17 calculated in this study. Furthermore, the strength ratio without applying the correction factor was 1.34 (a COV of 38%), suggesting that the inclusion of the correction factor in this study improved the accuracy of strength predictions.

Conclusion

In this study, a series of 24 structural experiments and a finite element method analysis were conducted to examine the use of strands as lifting loops. The following conclusions can be drawn from the results of the structural analysis and the experiments:

- The results of the FEA and pullout experiments confirmed that edge distance, embedment depth, and lifting angle are critical variables influencing the strength of the specimens.
- The specimens exhibited different failure modes depending on these key variables, which were classified as

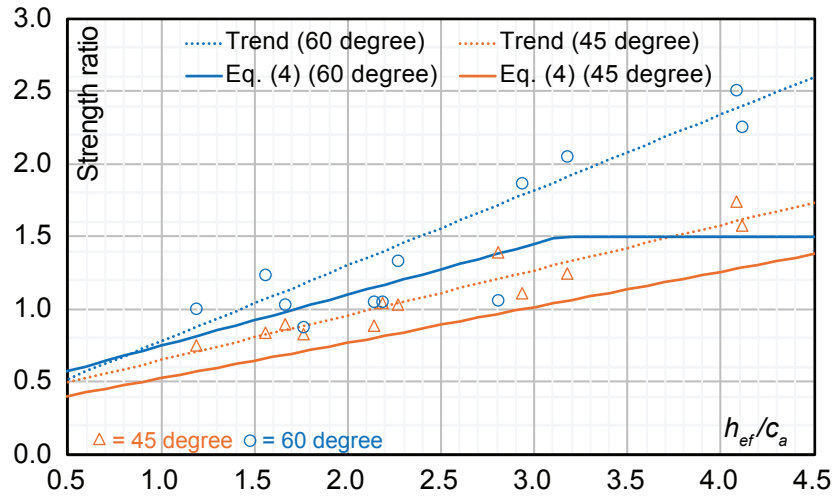

Figure 19. Comparison of trends with Eq. (4). Note: c_a = edge distance of strand lifting loops; h_{ef} = embedment depth of strand lifting loops.

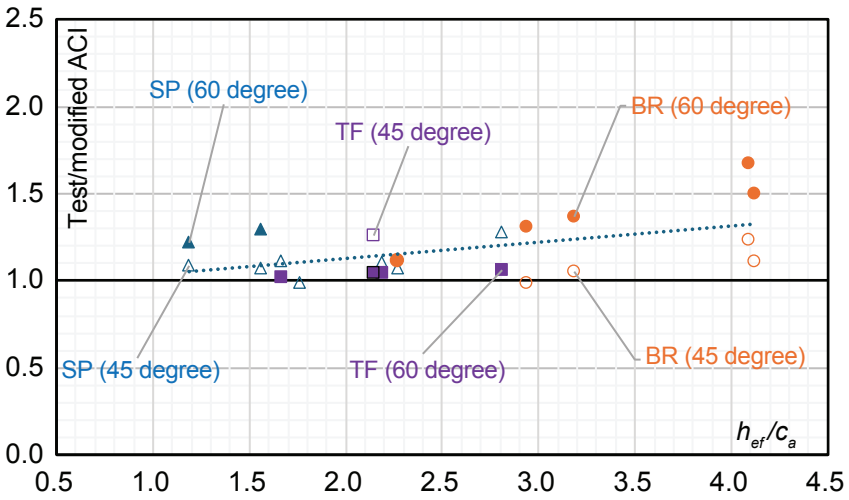

Figure 20. Comparison with tests from this study. Note: BR = breakout failure of the concrete; c_a = edge distance of strand lifting loops; h_{ef} = embedment depth of strand lifting loops; modified ACI = Building Code Requirements for Structural Concrete (ACI 318-19) and Commentary (ACI 318R-19) equations with modification factors from Eq. (3) or Eq. (4); SP = splitting rupture of the concrete; TF = tensile failure of the strand.

tensile failure (TF), concrete breakout failure (BR), and concrete splitting rupture (SP).

- When the influence factor h_{ef}/c_a was 3.0 or less, the specimens tended to fail in SP mode. When the influence factor exceeded 3.0, the specimens typically failed in BR mode.
- Tensile failure of the strand lifting loop (TF mode) occurred when the lifting angle was 60 degrees with an edge distance greater than or equal to 160 mm (6.3 in.) and an embedment depth greater than or equal to 350 mm (14 in.), or when the lifting angle was 45 degrees with an edge distance greater than or equal to 210 mm (8.3 in.) and an embedment depth greater than or equal to 450 mm (18 in.).
- The proposed equations, which apply modification factors to the ACI 318 design equations for anchors, accurately predicted the strength of the specimens.

This study is based on a limited number of specimens, so further research with a larger number of specimens is recommended. Additional areas for research could include the following:

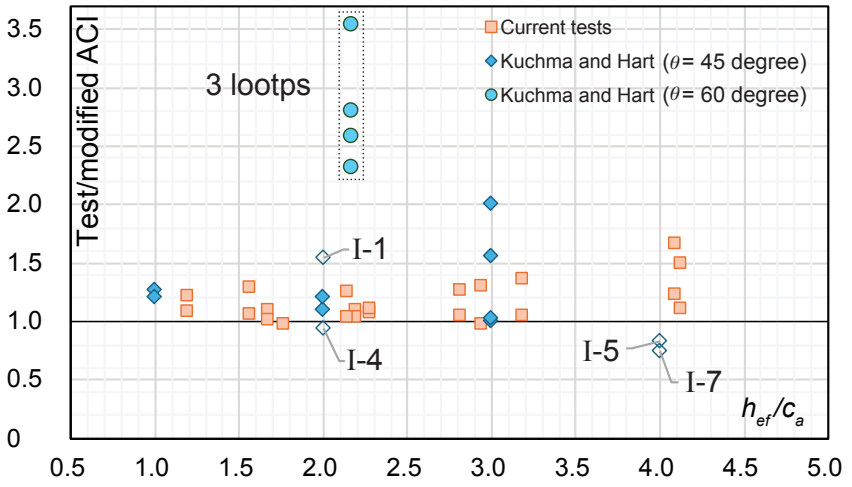

Figure 21. Comparison with test results including those from Kuchma and Hart (2009). Note: Kuchma and Hart = Kuchma and Hart (2009); modified ACI = Building Code Requirements for Structural Concrete (ACI 318-19) and Commentary (ACI 318R-19) equations with modification factors from Eq. (3) or Eq. (4); I-1 = test 1; I-4 = test 4; I-5 = test 5; I-7 = test 7; θ = lifting angle.

Table 4. Tests by Kuchma and Hart (2009)

Name	Lifting angle, degrees	Embedment depth h_{ef}, mm	Edge distance c_a, mm	Number of loops	Concrete strength, MPa	h_{ef}/c_a	Strength ratio
I-1	45	150	75	2	28.3	2.0	1.55
I-2			150		28.3	1.0	1.27
I-3			150		27.4	1.0	1.22
I-4			75		27.7	2.0	0.94
I-5	45	300	75	2	27.1	4.0	0.83
I-6			150		27.2	2.0	1.11
I-7			75		27.3	4.0	0.75
I-8			150		27.5	2.0	1.21
I-9		300	100	3	27.8	3.0	2.01
I-10					27.0	3.0	1.01
I-11					29.5	3.0	1.56
I-12					28.6	3.0	1.03
I-13	60	330	150	3	64.0	2.17	2.60
I-14					64.0	2.17	3.55
I-15					64.0	2.17	2.32
I-16					64.0	2.17	2.80

Note: 1 mm = 0.0394 in.; 1 MPa = 0.145 ksi.

- lifting loads at the demolding stage (with low concrete strength)
- multiple lifting loops
- the lifting angle at 90 degrees
- the evaluation and validation of experimental results through nonlinear FEA

Moreover, further studies are needed for cases that fall outside the scope of the experimental variables in this research.

References

1. PCI Industry Handbook Committee. 2017. *PCI Design Handbook: Precast and Prestressed Concrete*. MNL 120. 8th ed. Chicago, IL: PCI.

2. PCI Bridge Design Manual Steering Committee. 2023. *PCI Bridge Design Manual*. MNL 133. 4th ed. Chicago, IL: PCI.

3. ACI (American Concrete Institute) Committee 318. 2019. *Building Code Requirements for Structural Concrete (ACI 318-19) and Commentary (ACI 318R-19)*. Farmington Hills, MI: ACI.

4. Moustafa, S. 1974. *Pullout Strength of Strand and Lifting Loops*. Technical Bulletin 74-B5. Tacoma, WA: Concrete Technology Associates.

5. Kuchma, D. A., and C. R. Hart. 2009. *Development of Standard for Lifting Loops in Precast Deck Beams*. Research report ICT-09-056. Urbana, IL: Illinois Center for Transportation.

6. Chhetri, S., R. A. Chicchi, and A. E. Osborn. 2021. "Experimental Investigation of 0.6 in. Diameter Strand Lifting Loops." *PCI Journal* 66 (2): 71–87.

7. Chhetri, S., R. A. Chicchi, and S. J. Seguirant. 2020. "Industry Survey Results on the Use of Prestressing Strand Lifting Loops." *PCI Journal* 65 (4): 21–35.

8. Chhetri, S. and R. C. Cross. 2024. "Experimental Investigation of Multiple-Strand Lifting Loops." *PCI Journal* 69 (3): 74–88.

9. Cross, R. C. 2024. "Updates to Lifting Loops: Provisions and Research." *Aspire* (summer): 31–32.

Notation

A_{Nc} = projected concrete failure area of a single anchor or group of anchors, for calculation of strength in tension

A_{Nco} = projected concrete failure area of a single anchor for calculation of strength in tension if not limited by edge distance or spacing

A_{ps} = area of prestressing strand

$A_{se,N}$ = effective cross-sectional area of the anchor in tension

c_a = edge distance of strand lifting loops

f_{pu} = failure stress of strand

f_{uta} = specified tensile strength of anchor steel

h_{ef} = embedment depth of strand lifting loops

ℓ_{ext} = length of strand loop extension (bend)

N_b = basic concrete breakout strength

N_{cbg} = nominal concrete breakout strength in tension of a group of anchors

N_{sa} = nominal tensile strength for tensile failure of anchor steel

α = factor accounting for lifting angle of strand lifting loops in ACI anchor design

$\varepsilon_{c1,max}$ = maximum principal tensile strain

$\varepsilon_{c1,min}$ = minimum principal tensile strain

$\varepsilon_{c3,max}$ = maximum principal compressive strain

$\varepsilon_{c3,min}$ = minimum principal compressive strain

θ = lifting angle

$\sigma_{ps,max}$ = maximum stress in the strand

$\sigma_{ps,min}$ = minimum stress in the strand

$\sigma_{s',+max}$ = maximum tensile stress in the reinforcing bar

$\sigma_{s',-max}$ = minimum compressive stress in the reinforcing bar

Ψ_{β} = modification factors for using strand lifting loops in ACI anchor design

$\Psi_{c,N}$ = breakout cracking factor

$\Psi_{cp,N}$ = breakout splitting factor

$\Psi_{ec,N}$ = breakout eccentricity factor

$\Psi_{ed,N}$ = breakout edge effect factor

About the authors

Young-Hun Oh is a professor in the Department of Medical Space Design and Construction at Konyang University in Daejeon, South Korea.

Gang-Chul Lee is president of Onetop Engineering Co. in Seoul, South Korea.

HyunSup Noh is group leader of the Structural Technology Group at Samsung C & T Corp. in Seoul, South Korea.

Kyeong Woong Ra is a professional engineer in the Structural Technology Group at Samsung C & T Corp.

NanHee Lee is a professional engineer in the High-Tech Engineering Team at Samsung C & T Corp.

Jeong-Ho Moon is a professor emeritus of architectural engineering at Hannam University in Daejeon, South Korea, and director of the Research Institute of Onetop Engineering Co.

Abstract

This study investigates experiments and analyses related to the use of strand lifting loops for handling precast concrete members. To this end, a total of 24 specimens were prepared, with variables including edge distance, lifting angle, and embedment depth. A finite element analysis of the experimental conditions was conducted to validate the experimental method. In the experiments, each specimen was independently manufactured and tested under individually applied loads. The experimental results were analyzed in terms of the failure modes and strengths of the specimens with respect to the key variables. The results revealed that the failure modes of the specimens could be categorized into concrete splitting failure, concrete breakout failure, and strand tensile rupture, all of which were closely related to the influencing factor, embedment depth divided by edge distance. Based on the experimental results, modification factors for the design of strand lifting loops are proposed. The findings indicate that the predicted strengths, obtained by applying these modification factors to the anchor design equations from ACI 318, effectively reflect the effects of the key variables.

Keywords

Concrete failure, inclined load, strand lifting loop.

Review policy

This paper was reviewed in accordance with the Precast/Prestressed Concrete Institute's peer-review process. The Precast/Prestressed Concrete Institute is not responsible for statements made by authors of papers in PCI Journal. No payment is offered.

Publishing details

This paper appears in *PCI Journal* (ISSN 0887-9672) V. 70, No. 5, September–October 2025, and can be found at https://doi.org/10.15554/pcij70.5-03. *PCI Journal* is published bimonthly by the Precast/Prestressed Concrete Institute, 8770 W. Bryn Mawr Ave., Suite 1150, Chicago, IL 60631.

Reader comments

Please address any reader comments to *PCI Journal* editor-in-chief Tom Klemens at tklemens@pci.org or Precast/Prestressed Concrete Institute, c/o *PCI Journal*, 8770 W. Bryn Mawr Ave., Suite 1150, Chicago, IL 60631.